BMB Reports - Manuscript Submission

Manuscript Draft

Manuscript Number: BMB-21-126

Title: Reactive microglia and mitochondrial unfolded protein response following ventriculomegaly and behavior defects in kaolin-induced hydrocephalus

Article Type: Article

Keywords: hydrocephalus; UPRmt; microglia; neuroinflammation

Corresponding Author: Junyoung Heo

Authors: Jiebo Zhu[1,2,3,#], Min Joung Lee[1,2,3,#], Hee Jin Chang[1,4], Xianshu Ju[1,3], Jianchen Cui[1,3], Yu Lim Lee[1,3], Dahyun Go[1,2,3], Woosuk Chung[1,5,6], Eungseok Oh[1,4], Junyoung Heo[1,2,3,*]

Institution: [1]Department of Medical Science and [2]Department of Biochemistry and [3]Infection Control Convergence Research Center, Chungnam National University School of Medicine,
[4]Department of Neurology, Chungnam National University Hospital,
[5]Department of Anesthesiology and Pain Medicine, Chungnam National University School of Medicine,
[6]Department of Anesthesiology and Pain Medicine, Chungnam National University Hospital,

Manuscript Type: Article

Title: Reactive microglia and mitochondrial unfolded protein response following ventriculomegaly and behavior defects in kaolin-induced hydrocephalus

Jiebo Zhu[1,2,3,#], Min Joung Lee[1,2,3,#], Hee Jin Chang[1,4], Xianshu Ju[1,3], Jianchen Cui[1,3], Yu Lim Lee[1,3], Dahyun Go[1,2,3], Woosuk Chung[1,5,6], Eungseok Oh[1,4,*], Jun Young Heo[1,2,3,*]

[1]Department of Medical Science, Chungnam National University School of Medicine, South Korea

[2]Department of Biochemistry, Chungnam National University School of Medicine, South Korea

[3]Infection Control Convergence Research Center, Chungnam National University School of Medicine, South Korea

[4]Department of Neurology, Chungnam National University Hospital, South Korea

[5]Department of Anesthesiology and Pain Medicine, Chungnam National University School of Medicine, South Korea

[6]Department of Anesthesiology and Pain Medicine, Chungnam National University Hospital, South Korea

Running Title: Reactive microglia and UPRmt in hydrocephalus

Keywords: hydrocephalus, UPRmt, microglia, neuroinflammation

[*]Corresponding authors: Jun Young Heo, Tel: +82-42-580-8221; Fax: +82-42-580-8121; E-mail: junyoung3@gmail.com; Eungseok Oh, Tel: +82-42-280-7868; Fax: +82-42-252-8654; E-mail: doctor_oh@daum.net

[#] These authors have contributed equally to this work.

ABSTRACT

Ventriculomegaly induced by the abnormal accumulation of cerebrospinal fluid (CSF) leads to hydrocephalus, which is accompanied by neuroinflammation and mitochondrial oxidative stress. The mitochondrial stress activates mitochondrial unfolded protein response (UPRmt), which is essential for mitochondrial protein homeostasis. However, the association of inflammatory response and UPRmt in the pathogenesis of hydrocephalus is still unclear. To assess their relevance in the pathogenesis of hydrocephalus, we established a kaolin-induced hydrocephalus model in 8-week-old male C57BL/6J mice and evaluated it over time. We found that kaolin-injected mice showed prominent ventricular dilation, motor behavior defects at the 3-day, followed by the activation of microglia and UPRmt in the motor cortex at the 5-day. In addition, PARP-1/NF-κB signaling and apoptotic cell death appeared at the 5-day. Taken together, our findings demonstrate that activation of microglia and UPRmt occurs after hydrocephalic ventricular expansion and behavioral abnormalities which could be lead to apoptotic neuronal cell death, providing a new perspective on the pathogenic mechanism of hydrocephalus.

INTRODUCTION

Hydrocephalus is a common neurological disorder caused by abnormalities in cerebrospinal fluid (CSF) circulation and absorption, which results in the accumulation of CSF in the ventricular system and the dilation of ventricles (1). Increased CSF volume in ventricles generates shear stress, which leads to deformation of the ventricles and cortical thinning (2, 3). The dysregulation of the neuronal activity in the motor cortex is responsible for gait disturbances in patients with idiopathic normal pressure hydrocephalus (iNPH) (4). And, iNPH patient`s motor function can be recovered by CSF drainage, which is related to enhanced activity of frontal motor areas (5). Although the ventriculomegaly

correlated with motor deficits in kaolin-induced hydrocephalus rats, the underlying mechanisms are not yet clear (6).

Neuroinflammation-related biomarkers in CSF are increasingly being used to diagnose patients with hydrocephalus (7). Neuroinflammation and brain injury within the white matter of the corpus callosum, accompanied by the increased pro-inflammatory factors such as interleukin-6 (IL-6) and interleukin-1β (IL-1β) has been shown in the neonatal hydrocephalus model (8). The production of IL-6 and interleukin-8 (IL-8) were up-regulated in idiopathic hydrocephalus patients (9). Moreover, interleukin-10 (IL-10) and interleukin-33 (IL-33) in CSF can be used to monitor the hydrocephalus progression and the effectiveness of shunt surgery (10). In neuroinflammation, glial cells produce pro-inflammatory factors, such as tumor necrosis factor-α (TNF-α) and IL-6, that promote neuroinflammation and secondary brain damage (11). The increased expression of TNF-α is associated with periventricular white matter lesions and demyelination in patients with normal pressure hydrocephalus (NPH) (12). The neuroinflammatory changes caused by ventriculomegaly could be a trigger for neuronal damage in the brain, which eventually leads to behavioral and cognitive problems in iNPH (13). Nevertheless, little evidence has been provided in support of the relevance of neuroinflammation in hydrocephalus-related ventricular dilation and behavioral abnormalities.

Mitochondria have been considered to be responsible for stress adaptation response against external insult such as inflammation, oxidative stress that could be attenuated disease progression (14). The protective pathway that enhances stress resilience through the strengthening of mitochondrial function includes mitochondrial unfolded protein response (UPRmt) (15). To maintain the integrity of mitochondrial structure and function, UPRmt leads to the increase of the mitochondrial molecular chaperones and proteases expression such as heat shock protein 60 (HSP60), mitochondrial protease Lon protease (LONP1), and caseinolytic peptidase P (CLPP) (16) These molecules promote the recovery of the mitochondrial network to ensure optimal cellular function (17). Importantly, activated

UPRmt has been reported as a pathological feature of neurological diseases, including Alzheimer's disease (AD), Parkinson's disease (PD), Huntington's disease (HD), and amyotrophic lateral sclerosis (ALS) (18). Nevertheless, little evidence has been provided in support of the UPRmt is involved in hydrocephalus. We hypothesized that gliosis and the UPRmt are involved in the pathological process of hydrocephalus. Here, to test this hypothesis, we observed a kaolin-induced hydrocephalus mouse model over time, based on the well-established kaolin injection model described in rats (19). The elucidating for the involvement of UPRmt and gliosis in kaolin-injected mice would contribute to demonstrating a novel opinion on the pathogenesis of hydrocephalus.

RESULTS

Ventricular enlargement and neurobehavioral defects appear at the 3-day after kaolin injection

The pathological symptoms of hydrocephalus begin with ventricular dilation (20). Injection of kaolin into the cisterna magna resulted in disruption of CSF flow and an increase in ventricular size (21). To determine whether kaolin-injected mice developed hydrocephalus, we measured the size of the lateral ventricle (Lv), the dorsal part of the 3rd ventricle (d3v), the ventral part of the 3rd ventricle (v3v), and the 4th ventricle (4v), in the saline-treated group and 1-, 3-, 5-day kaolin-treated groups. There were no significant changes in the sizes of these ventricles in the 1-day group, but obvious ventricular enlargement in the 3-day and 5-day group, compared with the saline group (Fig. 1A–E). The size of the Lv, d3v, v3v, and 4v increased over 2-fold in the 3-day group, and more than 3-fold in the 5-day group, compared with the saline group (Fig. 1A–E). These results indicate that kaolin induces ventricular expansion starting at the 3-day, and continue expansion at the 5-day after injection.

The behavioral symptoms of hydrocephalus are associated with ventricular dilatation, such as shuffling gait (22). As we found a significant change of ventricular dilatation from the 3-day after kaolin injection, we assessed the behavior test in the 3-day group. We initially used the open-field test

to measure the mice's distance traveled for 10 min (23). We found saline-treated mice moved normally in the apparatus, but kaolin-treated mice showed difficulty walking and traveled distance 60% shorter than the saline group (Fig. 1F, G).

To verify whether the hypokinetic movement in kaolin mice is correlated with neurologic dysfunction, we evaluated the differences in neurobehavioral function between saline and 3-day groups, according to the modified neurological score (24). In the 3-day group, 75% of the mice showed decreased scavenging and scatter reflexes, indicative of neurological dysfunction (Fig. 1H). We next performed a horizontal grid test to examine the muscle strength and motor ability of kaolin mice, by analyzing hang time, successful steps, and total steps (25). Compared with saline mice, kaolin mice showed that the average hang time was reduced by 75% (Fig. 1I), the number of successful steps and total steps was decreased by ~90% (Fig. 1J, K), and the percentage of successful steps was approximately halved (Fig. 1L). Taken together, these results showed that locomotor ability and muscular strength prominently are reduced with ventricular enlargement at the 3-day.

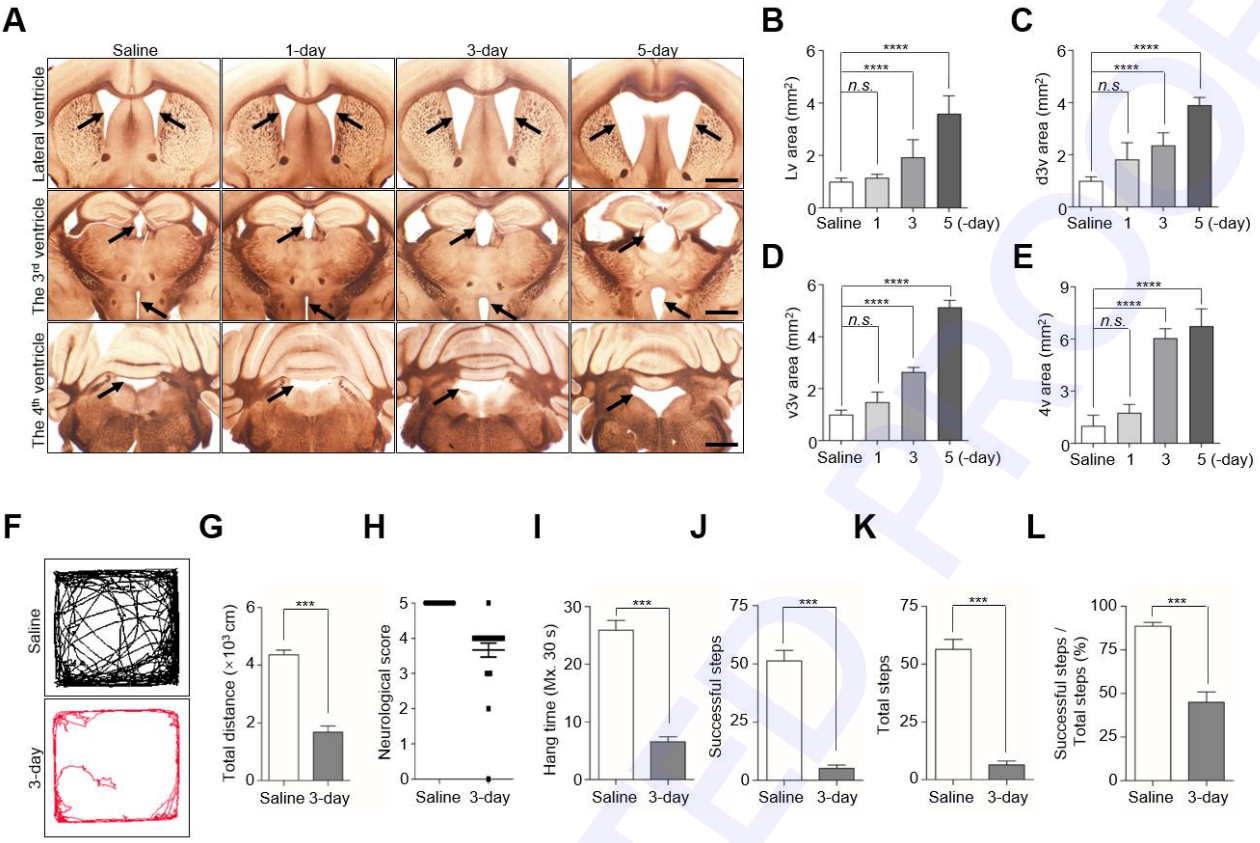

Microglia activates at the 5-day after kaolin injection

In the kaolin-induced hydrocephalic rats, neuroinflammation and microglial reaction followed by ventricular enlargement (26). Moreover, the expression of the inflammatory factor TNF-α is increased in the CSF of NPH patients (12). To investigate whether microglia and TNF-α increase in our kaolin-induced hydrocephalic mice, we monitored the expression of the microglia marker Iba-1, and inflammatory factor, TNF-α in the motor cortex. Microglia in the kaolin group exhibited an altered morphology, characterized by an enlarged cell body and a “bushier” appearance, accompanied by the expression of TNF-α up-regulated in the 5-day group, compared with the saline group (Fig. 2A). Immunofluorescence staining showed that the expression of Iba-1 increased 2.3-fold, with TNF-α staining intensity increased by 1.5-fold in the 5-day group, compared with the saline group (Fig. 2B, C).

In addition, Iba-1 protein levels also increased ~12-fold, accompanied by a 1.6-fold increase in TNF-α in the 5-day group, compared with the saline group, whereas Iba-1 and TNF-α protein levels in the 1- and 3-day groups showed no significant changes compared with the saline group (Fig. 2D–F). Consistently, TNF-α levels in brain tissue lysates, determined by ELISA, increased 1.5-fold in the 5-day group, compared with the saline group (Fig. 2G). These results suggest that inflammatory response occurs after the enlargement of the ventricle in the kaolin-induced hydrocephalic mice.

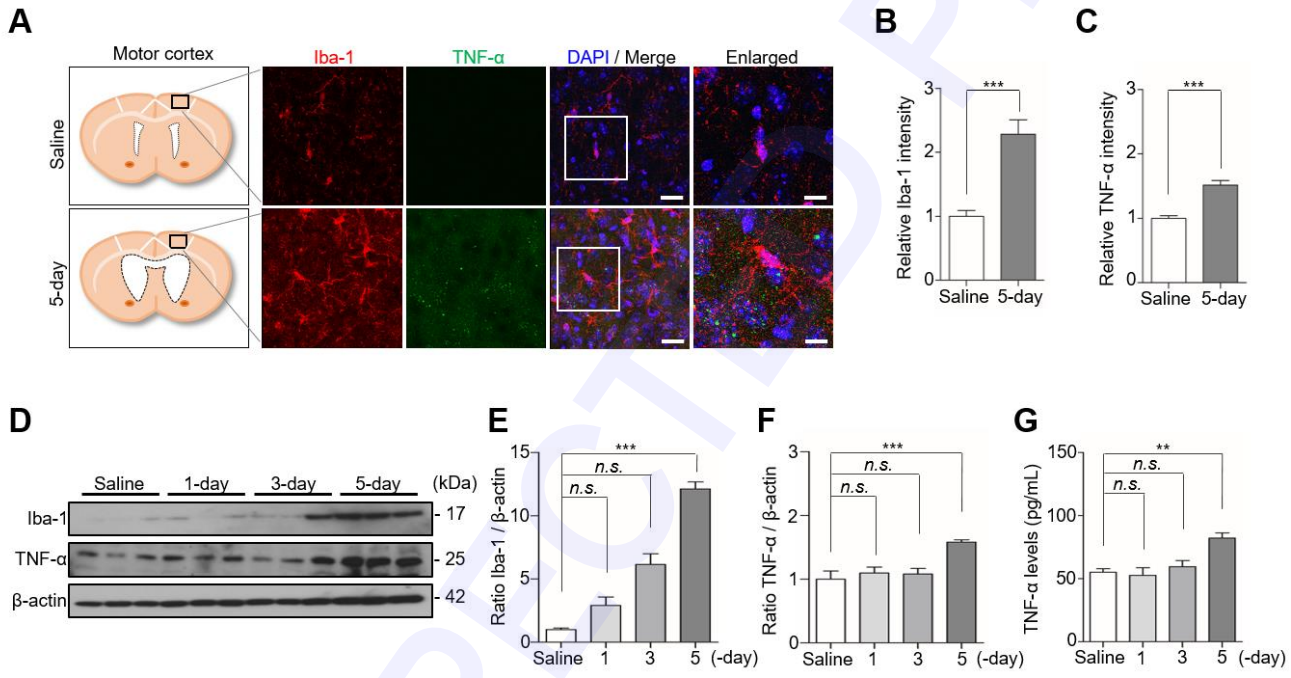

Apoptotic neuronal cell death occurs in the motor cortex at the 5-day after kaolin injection

Microglia promote the release of inflammatory cytokine TNF-α, resulting in progressive neuronal cell death (27). Furthermore, nuclear factor kappa B (NF-κB) is coactivated with poly (ADP-ribose) polymerase-1 (PARP-1), which participates in cell death in microgliosis (28). Therefore, to examine neuronal cell death under the condition of increased TNF-α in kaolin-injected mice, we assessed the expression of PARP-1 and cleaved PARP-1, as well as NF-κB p65 and phospho-NF-κB p65, the hub subunit of NF-κB, in the motor cortex (29). This analysis showed that compared with the saline group, mice in the 5-day group showed a 3.1-fold increase in PARP-1 expression, a 1.5-fold increase in

cleaved PARP-1 (Fig. 3A–C), a 1.7-fold increase in NF-κB p65, and 1.4-fold increase phospho-NF-κB p65 (Fig. 3D–F). By contrast, none of these proteins exhibited a change in expression in 1-day or 3-day groups. Using TUNEL staining and Nissl staining, we observed the number of neuronal cells decreased in the 5-day group compared with the saline group (Supplemental fig. 1). Collectively, these results suggest that coactivated PARP-1 and NF-κB are involved in the neuronal apoptosis that occurred at 5-day after kaolin injection.

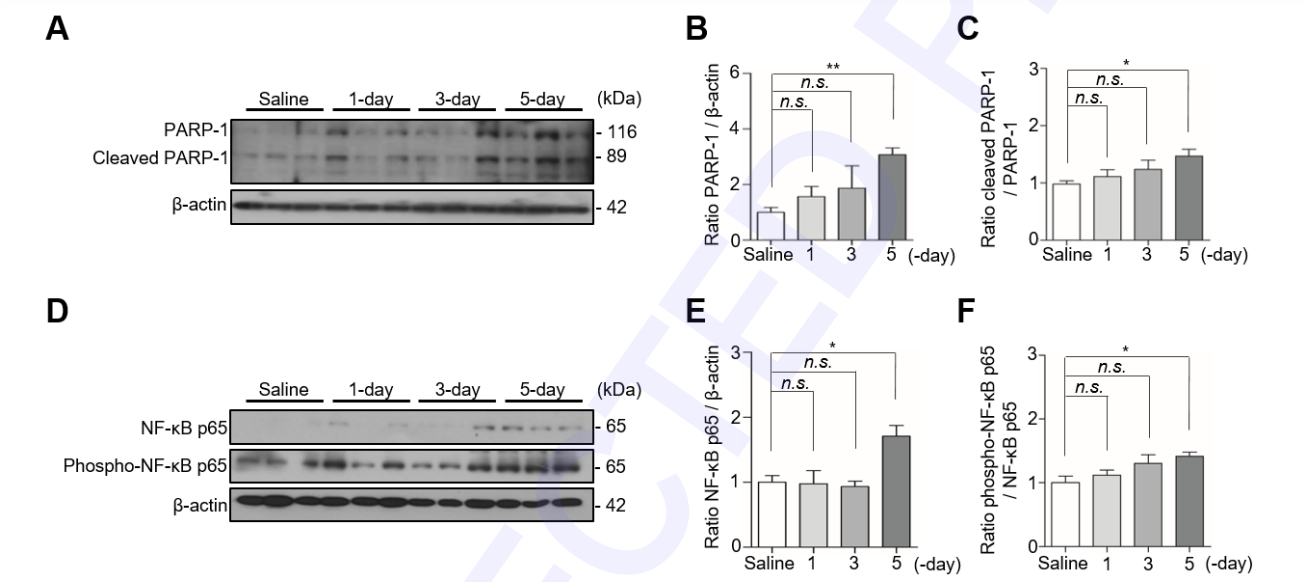

UPRmt activates at the 5-day after kaolin injection

Both neuroinflammation and mitochondrial dysfunction are crucial pathomechanisms in neurological diseases (30). During mitochondrial dysfunction, cells activate several defense mechanisms that serve to maintain optimal cellular function, in particular, UPRmt (15). To determine whether the UPRmt is activated in kaolin-injected mice, we assessed the expression of mitochondrial molecular chaperones and proteases LONP1, HSP60, and CLPP (17). The expression of three proteins was significantly increased in the 5-day group compared with the saline group, with LONP1 increasing 1.9-fold (Fig. 4A, B), HSP60 increasing 3-fold (Fig. 4A, C), and CLPP increasing 3.9-fold (Fig. 4A, D). Consistent with the protein results, the transcriptional level of *Lonp1*, *Hspd1*, and *Clpp* roughly increased 2-fold

in the 5-day group compared with the saline group (Fig. 4E–G). Taken together, our results demonstrate that activation of microglia and UPRmt in the motor cortex are following hydrocephalic ventricular expansion and behavioral abnormalities, that could contribute the apoptotic neuronal cell death.

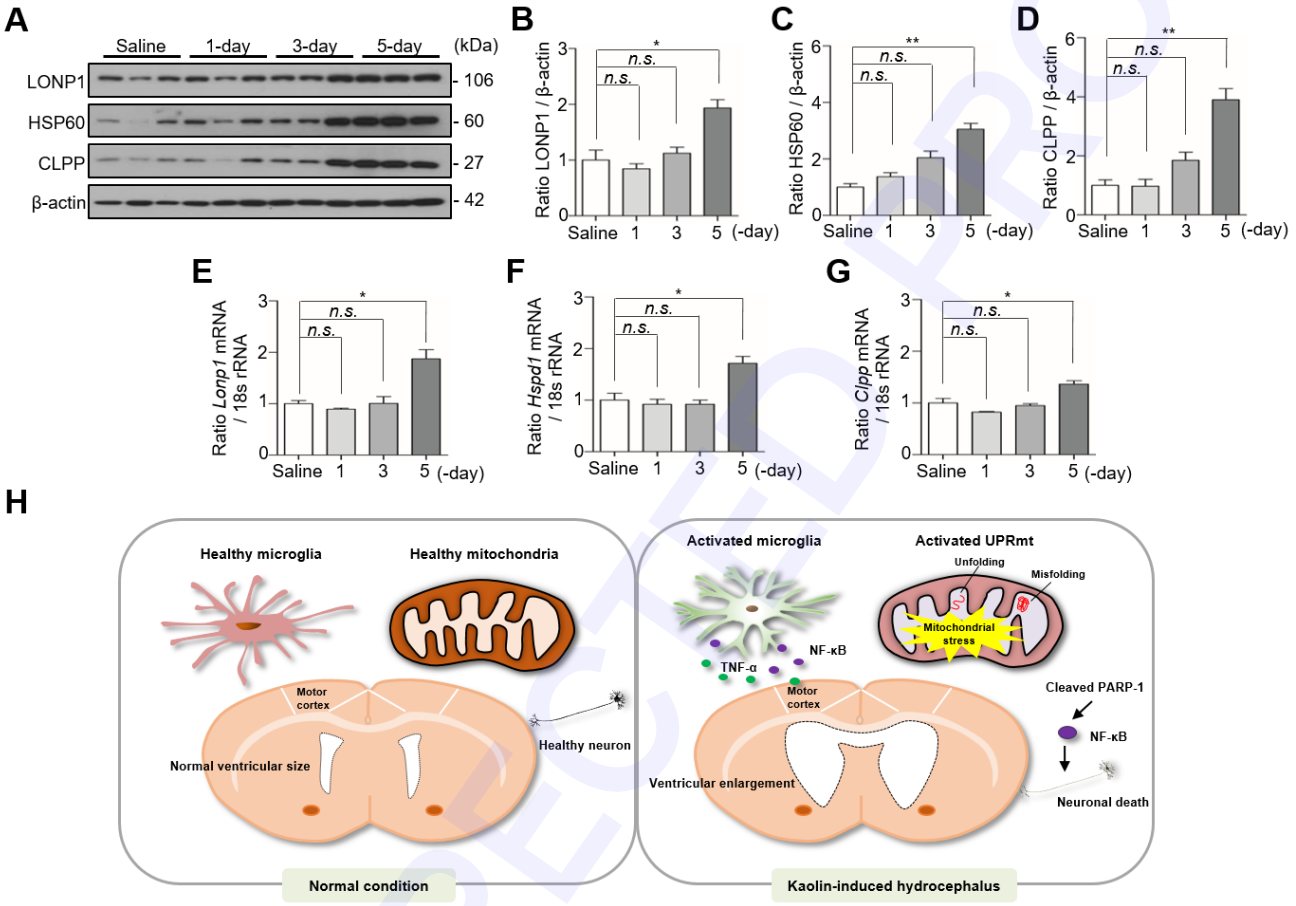

DISCUSSION

Hydrocephalic patients show behavioral abnormalities with abnormal accumulation of CSF in ventricles (1). In addition, inflammatory cytokines such as TNF-α, IL-1β, IL-6 were suggested as the biomarkers of NPH patients because the cytokines increased in CSF of NPH patients (31). However, the association between neuroinflammatory response and behavior symptoms as well as the mechanism underlying the ventricular enlargement that may induce behavior defects are still unclear. Kaolin (aluminum silicate) has been used to generate hydrocephalus by direct cisterna magna injection in

157 animal models (32). The kaolin-induced hydrocephalus is a well-established animal hydrocephalus
158 model, to study the pathogenesis of hydrocephalus (33). Kaolin was localized to the fourth ventricle
159 by the cisterna magna injection, the obstructive hydrocephalus was expected to develop within seven
160 days after induction (19). Many researchers have been reported that ventricular dilation, behavioral
161 defects, and neuroinflammation in the kaolin-induced hydrocephalus model (34-36). However, the
162 mitochondria-related pathogenesis in the kaolin-induced hydrocephalus model is not fully understood.
163 In the present study, we sequentially investigated the symptoms of the kaolin-induced hydrocephalus
164 mice over time after the injection of kaolin. We observed enlarged ventricle and behavior defects at
165 the 3-day after that time, microglia activated and TNF-α level increased at the 5-day after kaolin
166 injection. We also demonstrated that UPRmt were induced at the 5-day when inflammatory response
167 occurred with apoptotic neuronal cell death in the kaolin-induced hydrocephalus mice.

168 Reactive microglia serve as a potential pathogenic mechanism for neonatal hydrocephalus (37).
169 Activation of microglia in the white matter is related to ventricular dilatation (6). After the change to
170 reactive microglia by ventriculomegaly, it starts to release the inflammatory mediator TNF-α, which
171 can provide a positive feedback loop to spread the inflammatory reaction around the microenvironment
172 which is called gliosis (38). TNF-α was correlated with the severity of congenital hydrocephalic mice
173 (12, 39, 40). Similarly, the level of TNF-α in CSF is positively correlated with the severity of NPH
174 patients, and drainage surgery can not only improve the clinical symptoms of hydrocephalus but also
175 completely reduce the secretion of TNF-α (12). The presence of TNF-α could explain the reactive
176 gliosis is closely associated with the severity of ventricular dilation in hydrocephalic rats (35).
177 Consistent with our findings, inflammatory responses result from ventricle enlargement in the
178 hydrocephalic brain. Although we investigated microglia activation by observing morphological
179 changes of microglia and increase of Iba-1 expression, we can not find a profound change of astrocyte
180 within 5-days in the kaolin-induced hydrocephalic mice (Supplemental fig. 2), unlike in the

hydrocephalic rat model (35). Astrocyte alteration needs to be in further investigation in the hydrocephalus mice over time.

In neurodegenerative diseases, glia-mediated neuroinflammation aggravates neuronal degeneration and increases neuronal cell death (41, 42). PARP-1 acts as the coactivator of NF-κB, which plays a crucial role in inflammatory disorders (43). Furthermore, PARP-1 promotes DNA repair, cleaved PARP-1 initiates the apoptotic cell death pathway (44). In a mouse model of traumatic brain injury (TBI), PARP-1 induces neuronal cell death through microglial activation (45). These reports indicate that neuronal cell death is related to microglial activation by the PARP-1/NF-κB signaling pathway. Consistent with these results, the expression of PARP-1, cleaved PARP-1, and NF-κB is increased at the 5-day after kaolin injection, suggesting the presence of apoptotic neurons in kaolin-treated mice. Although we labeled broken DNA strands in the motor cortex using TUNEL staining, which is a well-known assay of neuronal apoptosis, axonal damage-associated molecules, such as neurofilament light (NFL) and total-tau (T-tau) in kaolin mice need to be further investigated (46).

Mitochondrial oxidative stress is the common feature of chronic neurodegenerative diseases (47). Mitochondrial oxidative phosphorylation (OXPHOS) dysfunction produces reactive oxygen species (ROS), which mediates neuronal dysfunction and aggravates perinatal hydrocephalus (14, 48). During mitochondrial and cellular dysfunction, mitochondrial stress responses intervene to rebuild correct protein and maintain cellular homeostasis, UPRmt. This pathway mediates the adaptative responses against microenvironmental stimuli (49). In the case of Surf1 (-/-) mice which showed reduced cytochrome *c* oxidase (CcO) activity, UPRmt might contribute to the enhancement of stress adaptation response by increased expression of UPRmt components CLPP, HSP60, and LONP1 (50). We also found that LONP1, HSP60, and CLPP protein expression and mRNA level increased at the 5-day after kaolin injection when inflammatory response upregulated. Taken together, we demonstrated that inflammatory response and UPRmt activation simultaneously occurred with neuronal cell death after

ventricular enlargement. Although we assumed that UPRmt progresses neuronal cell death by observing apoptotic neuronal cells, the role of UPRmt that may induce or alleviate apoptosis remains unclear and require further investigation.

In conclusion, kaolin-induced hydrocephalus mice showed prominent dilation of ventricles and motor behavior defects at the 3-day. The inflammatory response such as microglia activation and increase of TNF-α occurred with PARP-1/NF-κB signaling and UPRmt upregulation at the 5-day. By demonstrating that activated microglia and UPRmt are following hydrocephalic ventricular expansion and behavioral abnormalities, our findings provide new insights into the pathogenic mechanism of hydrocephalus (Fig. 4H).

MATERIALS AND METHODS

Materials and methods are available in the supplemental material.

ACKNOWLEDGEMENTS

This research was supported by the Ministry of Science, ICT (grant number NRF-2017R1A5A2015385, 2019M3E5D1A02068575, 2019R1F1A1059586).

CONFLICTS OF INTEREST

The authors have no conflicting interests.

FIGURE LEGENDS

Fig. 1. Kaolin-induced hydrocephalus mice show ventricular enlargement and motor disturbances. (A) Coronal sections showed ventricles saline and 1, 3, 5-day after kaolin injection. (B–E) Bar plots were showed the Lv, d3v, v3v, and 4v areas. Black arrowheads indicate the ventricles, in the 3v figures, the arrowheads represent the d3v (top) and the v3v (bottom). (F, G) Movement activity was measured for

226 10 min in the open-field test. (H) The neurological function was scored by a 5-point paradigm and
227 plotted. (I–L) Bar plots showed the results were calculated for 30 s in a horizontal grid test. Bregma in
228 Lv (+0.14 mm), in 3v (-1.12 mm ~ -1.46 mm), in 4v (-5.88 mm). Ventricles size (n = 6), behavior test
229 (n (saline) = 16, n (3-day) = 24 for the neurological score, n (3-day) = 23 for the open-field test and
230 horizontal grid test, ** P < 0.01, *** P < 0.001; n.s., not significant). Scale bar: A: 200 μm.

231 **Fig. 2.** Kaolin-induced hydrocephalus mice activate microglia at the 5-day. (A) The motor cortex was
232 stained for Iba-1 (red) and TNF-α (green). (B, C) The immunofluorescence intensity of Iba-1 and TNF-
233 α was quantified. (D) The expression of Iba-1 and TNF-α in the motor cortex was analyzed by western
234 blotting. (E, F) The intensity value of Iba-1 and TNF-α was shown. (G) The TNF-α level was analyzed
235 by ELISA. Western blotting (n = 3, from three independent samples performed twice independently),
236 immunofluorescence and ELISA (n = 6, ** P < 0.01, *** P < 0.001; n.s., not significant). Scale bar:
237 A: 20 μm, the enlarged images: 10 μm.

238 **Fig. 3.** Kaolin-induced hydrocephalus mice show neuronal apoptosis associated with PARP-1 and NF-
239 κB up-regulated at the 5-day. (A) The protein expression of PARP-1 and cleaved PARP-1 in the motor
240 cortex were analyzed by western blotting. (B, C) The intensity value of PARP-1 and cleaved PARP-1
241 was shown. (D) The expression of NF-κB p65 and phospho-NF-κB p65 in the motor cortex were
242 analyzed by western blotting. (E, F) The intensity value of NF-κB p65 and phospho-NF-κB p65 was
243 shown. PARP-1 and NF-κB p65 proteins levels were normalized to β-actin, cleaved PARP-1 protein
244 level was normalized to PARP-1, and phospho-NF-κB p65 protein level was normalized to NF-κB p65.
245 (n = 3, from three independent samples performed twice independently, * P < 0.05, ** P < 0.01; n.s.,
246 not significant).

247 **Fig. 4.** Kaolin-induced hydrocephalus mice activate UPRmt at the 5-day. (A) The expression of
248 LONP1, HSP60, and CLPP in the motor cortex was analyzed by western blotting. (B–D) The intensity

value of LONP1, HSP60, and CLPP was shown. (E–G) The expression of *Lonp1*, *Hspd1*, and *Clpp* in the motor cortex was analyzed by qPCR. Western blotting (n = 3, from three independent samples performed twice independently), qPCR n = 6 (* $P < 0.05$, ** $P < 0.01$; n.s., not significant). (H) The schematic represents the presence of microglia and UPRmt in the motor cortex are following hydrocephalic ventricular expansion and behavioral abnormalities.

REFERENCES

1. Kahle KT, Kulkarni AV, Limbrick DD, Jr. and Warf BC (2016) Hydrocephalus in children. Lancet 387, 788-799

2. Levine DN (2008) Intracranial pressure and ventricular expansion in hydrocephalus: have we been asking the wrong question? J Neurol Sci 269, 1-11

3. Ferris CF, Cai X, Qiao J et al (2019) Life without a brain: Neuroradiological and behavioral evidence of neuroplasticity necessary to sustain brain function in the face of severe hydrocephalus. Sci Rep 9, 16479

4. Chistyakov AV, Hafner H, Sinai A, Kaplan B and Zaaroor M (2012) Motor cortex disinhibition in normal-pressure hydrocephalus. J Neurosurg 116, 453-459

5. Lenfeldt N, Larsson A, Nyberg L et al (2008) Idiopathic normal pressure hydrocephalus: increased supplementary motor activity accounts for improvement after CSF drainage. Brain 131, 2904-2912

6. Olopade FE, Shokunbi MT and Sirén AL (2012) The relationship between ventricular dilatation, neuropathological and neurobehavioural changes in hydrocephalic rats. Fluids Barriers CNS 9, 19

7. Harris CA, Morales DM, Arshad R, McAllister JP, 2nd and Limbrick DD, Jr. (2021) Cerebrospinal fluid biomarkers of neuroinflammation in children with hydrocephalus and shunt malfunction. Fluids Barriers CNS 18, 4

8. Goulding DS, Vogel RC, Pandya CD et al (2020) Neonatal hydrocephalus leads to white matter neuroinflammation and injury in the corpus callosum of Ccdc39 hydrocephalic mice. J Neurosurg Pediatr, 1-8

9. Czubowicz K, Głowacki M, Fersten E, Kozłowska E, Strosznajder RP and Czernicki Z (2017) Levels of selected pro- and anti-inflammatory cytokines in cerebrospinal fluid in patients with hydrocephalus. Folia Neuropathol 55, 301-307

10. Sosvorova L, Mohapl M, Vcelak J, Hill M, Vitku J and Hampl R (2015) The impact of selected cytokines in the follow-up of normal pressure hydrocephalus. Physiol Res 64, S283-290

11. Gaire BP and Choi JW (2021) Critical Roles of Lysophospholipid Receptors in Activation of Neuroglia and Their Neuroinflammatory Responses. Int J Mol Sci 22

12. Tarkowski E, Tullberg M, Fredman P and Wikkelsö C (2003) Normal pressure hydrocephalus triggers intrathecal production of TNF-alpha. Neurobiol Aging 24, 707-714

13. Wang Z, Zhang Y, Hu F, Ding J and Wang X (2020) Pathogenesis and pathophysiology of idiopathic normal pressure hydrocephalus. CNS Neurosci Ther 26, 1230-1240

14. Chen Y, Zhou Z and Min W (2018) Mitochondria, Oxidative Stress and Innate Immunity. Front Physiol 9, 1487

15. Melber A and Haynes CM (2018) UPR(mt) regulation and output: a stress response mediated by mitochondrial-nuclear communication. Cell Res 28, 281-295

16. Sorrentino V, Menzies KJ and Auwerx J (2018) Repairing Mitochondrial Dysfunction in Disease. Annu Rev Pharmacol Toxicol 58, 353-389

17. Shpilka T and Haynes CM (2018) The mitochondrial UPR: mechanisms, physiological functions and implications in ageing. Nat Rev Mol Cell Biol 19, 109-120

18. Shen Y, Ding M, Xie Z et al (2019) Activation of Mitochondrial Unfolded Protein Response in SHSY5Y Expressing APP Cells and APP/PS1 Mice. Front Cell Neurosci 13, 568

19. Collins P (1979) Experimental obstructive hydrocephalus in the rat: a scanning electron microscopic study. Neuropathol Appl Neurobiol 5, 457-468

20. Schob S, Weiß A, Dieckow J et al (2016) Correlations of Ventricular Enlargement with Rheologically Active Surfactant Proteins in Cerebrospinal Fluid. Front Aging Neurosci 8, 324

21. Basati S, Desai B, Alaraj A, Charbel F and Linninger A (2012) Cerebrospinal fluid volume measurements in hydrocephalic rats. J Neurosurg Pediatr 10, 347-354

22. Solana E, Poca MA, Sahuquillo J, Benejam B, Junqué C and Dronavalli M (2010) Cognitive and motor improvement after retesting in normal-pressure hydrocephalus: a real change or merely a learning effect? J Neurosurg 112, 399-409

23. Osmon KJ, Vyas M, Woodley E, Thompson P and Walia JS (2018) Battery of Behavioral Tests Assessing General Locomotion, Muscular Strength, and Coordination in Mice. J Vis Exp

24. Bloch O, Auguste KI, Manley GT and Verkman AS (2006) Accelerated progression of kaolin-induced hydrocephalus in aquaporin-4-deficient mice. J Cereb Blood Flow Metab 26, 1527-1537

25. Kim ST, Son HJ, Choi JH, Ji IJ and Hwang O (2010) Vertical grid test and modified horizontal grid test are sensitive methods for evaluating motor dysfunctions in the MPTP mouse model of Parkinson's disease. Brain Res 1306, 176-183

26. Khan OH, Enno TL and Del Bigio MR (2006) Brain damage in neonatal rats following kaolin induction of hydrocephalus. Exp Neurol 200, 311-320

27. Spagnuolo C, Moccia S and Russo GL (2018) Anti-inflammatory effects of flavonoids in neurodegenerative disorders. Eur J Med Chem 153, 105-115

28. Gisslen T, Ennis K, Bhandari V and Rao R (2015) Recurrent hypoinsulinemic hyperglycemia in neonatal rats increases PARP-1 and NF-κB expression and leads to microglial activation in the cerebral cortex. Pediatr Res 78, 513-519

29. Pan Z, Yang K, Wang H et al (2020) MFAP4 deficiency alleviates renal fibrosis through inhibition of NF-κB and TGF-β/Smad signaling pathways. Faseb j 34, 14250-14263

30. Harland M, Torres S, Liu J and Wang X (2020) Neuronal Mitochondria Modulation of LPS-Induced Neuroinflammation. J Neurosci 40, 1756-1765

31. Sosvorova L, Kanceva R, Vcelak J et al (2015) The comparison of selected cerebrospinal fluid and serum cytokine levels in patients with multiple sclerosis and normal pressure hydrocephalus. Neuro Endocrinol Lett 36, 564-571

32. Duru S, Oria M, Arevalo S et al (2019) Comparative study of intracisternal kaolin injection techniques to induce congenital hydrocephalus in fetal lamb. Childs Nerv Syst 35, 843-849

33. Silverberg GD, Miller MC, Pascale CL et al (2015) Kaolin-induced chronic hydrocephalus accelerates amyloid deposition and vascular disease in transgenic rats expressing high levels of human APP. Fluids Barriers CNS 12, 2

34. Shim I, Ha Y, Chung JY, Lee HJ, Yang KH and Chang JW (2003) Association of learning and memory impairments with changes in the septohippocampal cholinergic system in rats with kaolin-induced hydrocephalus. Neurosurgery 53, 416-425; discussion 425

35. Xu H, Zhang SL, Tan GW et al (2012) Reactive gliosis and neuroinflammation in rats with communicating hydrocephalus. Neuroscience 218, 317-325

36. Olopade FE, Shokunbi MT, Azeez IA, Andrioli A, Scambi I and Bentivoglio M (2019) Neuroinflammatory Response in Chronic Hydrocephalus in Juvenile Rats. Neuroscience 419, 14-22

37. Wu KY, Tang FL, Lee D et al (2020) Ependymal Vps35 Promotes Ependymal Cell Differentiation and Survival, Suppresses Microglial Activation, and Prevents Neonatal Hydrocephalus. J Neurosci 40, 3862-3879

38. Brás JP, Bravo J, Freitas J et al (2020) TNF-alpha-induced microglia activation requires miR-342: impact on NF-kB signaling and neurotoxicity. Cell Death Dis 11, 415

39. Takase H, Chou SH, Hamanaka G et al (2020) Soluble vascular endothelial-cadherin in CSF after subarachnoid hemorrhage. Neurology 94, e1281-e1293

40. Jiménez AJ, Rodríguez-Pérez LM, Domínguez-Pinos MD et al (2014) Increased levels of tumour necrosis factor alpha (TNFα) but not transforming growth factor-beta 1 (TGFβ1) are associated with the severity of congenital hydrocephalus in the hyh mouse. Neuropathol Appl Neurobiol 40, 911-932

41. Joshi AU, Minhas PS, Liddelow SA et al (2019) Fragmented mitochondria released from microglia trigger A1 astrocytic response and propagate inflammatory neurodegeneration. Nat Neurosci 22, 1635-1648

42. Hirsch EC and Hunot S (2009) Neuroinflammation in Parkinson's disease: a target for neuroprotection? Lancet Neurol 8, 382-397

43. Hassa PO and Hottiger MO (2002) The functional role of poly(ADP-ribose)polymerase 1 as novel coactivator of NF-kappaB in inflammatory disorders. Cell Mol Life Sci 59, 1534-1553

359 44. Malhotra U, Zaidi AH, Kosovec JE et al (2013) Prognostic value and targeted inhibition of
360 survivin expression in esophageal adenocarcinoma and cancer-adjacent squamous epithelium.
361 PLoS One 8, e78343

362 45. Stoica BA, Loane DJ, Zhao Z et al (2014) PARP-1 inhibition attenuates neuronal loss,
363 microglia activation and neurological deficits after traumatic brain injury. J Neurotrauma 31,
364 758-772

365 46. Niu LD, Xu W, Li JQ et al (2019) Genome-wide association study of cerebrospinal fluid
366 neurofilament light levels in non-demented elders. Ann Transl Med 7, 657

367 47. Fischer R and Maier O (2015) Interrelation of oxidative stress and inflammation in
368 neurodegenerative disease: role of TNF. Oxid Med Cell Longev 2015, 610813

369 48. Delavallée L, Mathiah N, Cabon L et al (2020) Mitochondrial AIF loss causes metabolic
370 reprogramming, caspase-independent cell death blockade, embryonic lethality, and perinatal
371 hydrocephalus. Mol Metab 40, 101027

372 49. D'Amico D, Sorrentino V and Auwerx J (2017) Cytosolic Proteostasis Networks of the
373 Mitochondrial Stress Response. Trends Biochem Sci 42, 712-725

374 50. Pharaoh G, Pulliam D, Hill S, Sataranatarajan K and Van Remmen H (2016) Ablation of the
375 mitochondrial complex IV assembly protein Surf1 leads to increased expression of the
376 UPR(MT) and increased resistance to oxidative stress in primary cultures of fibroblasts. Redox
377 Biol 8, 430-438

378

Figure 1

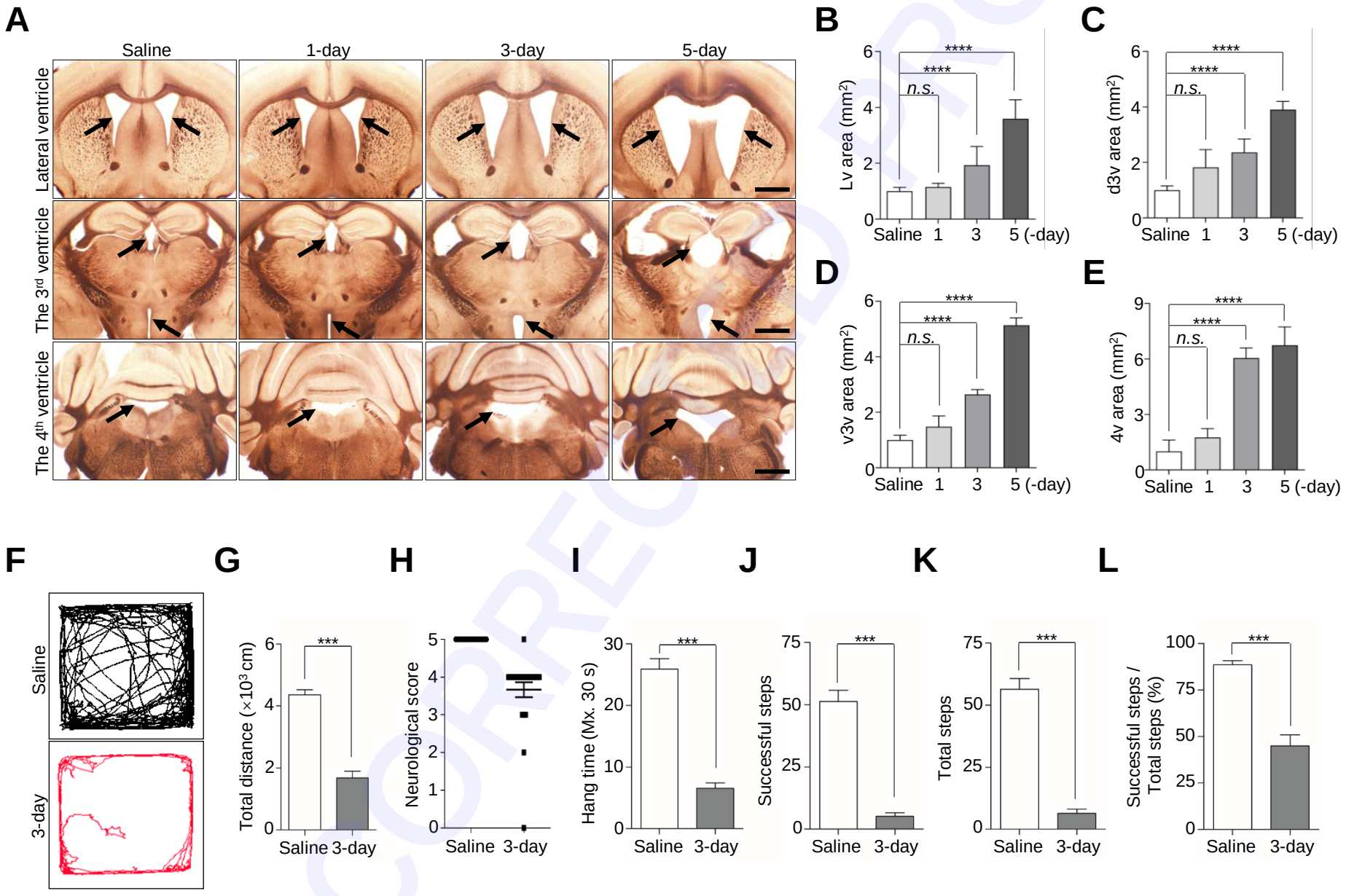

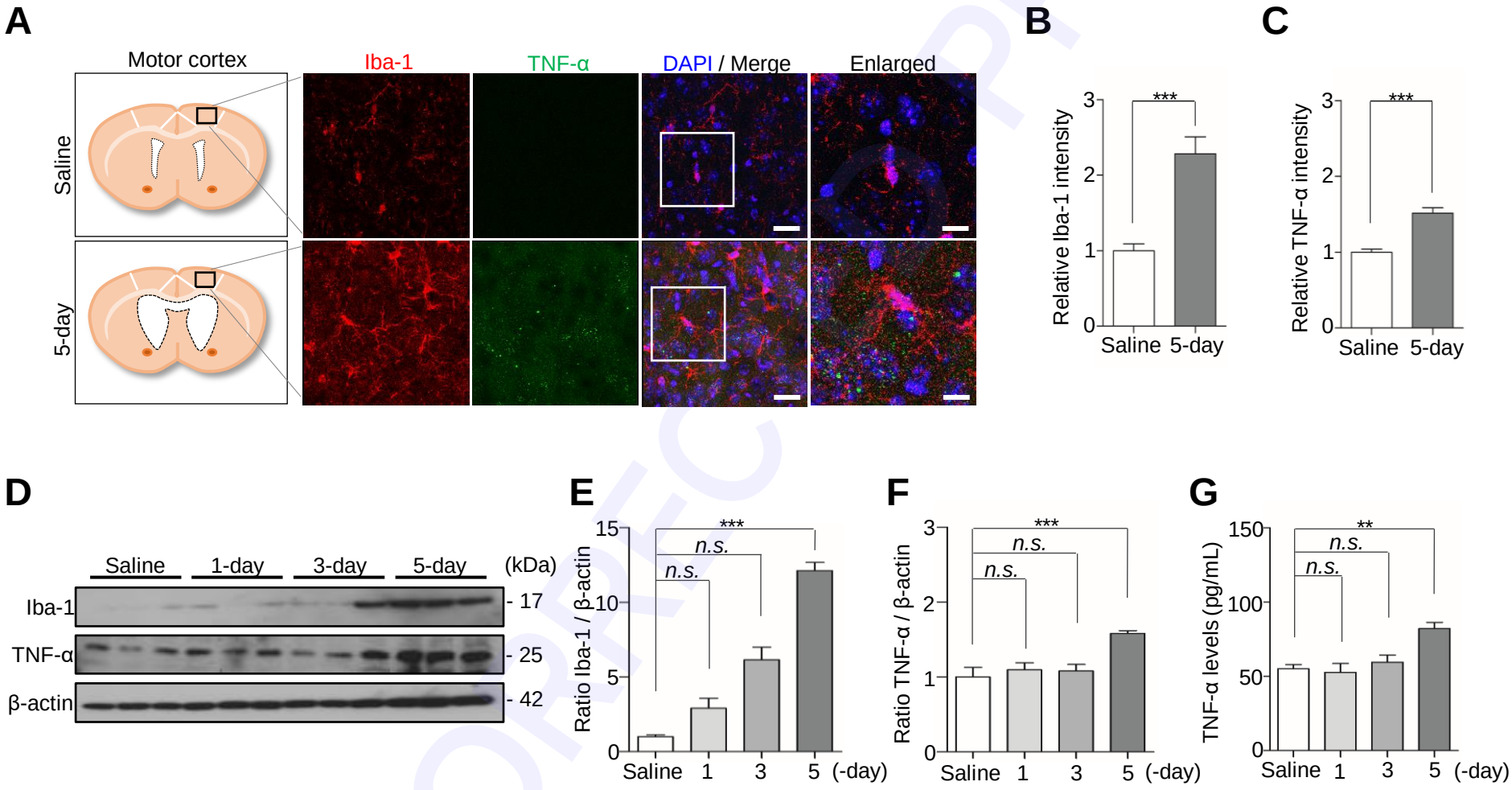

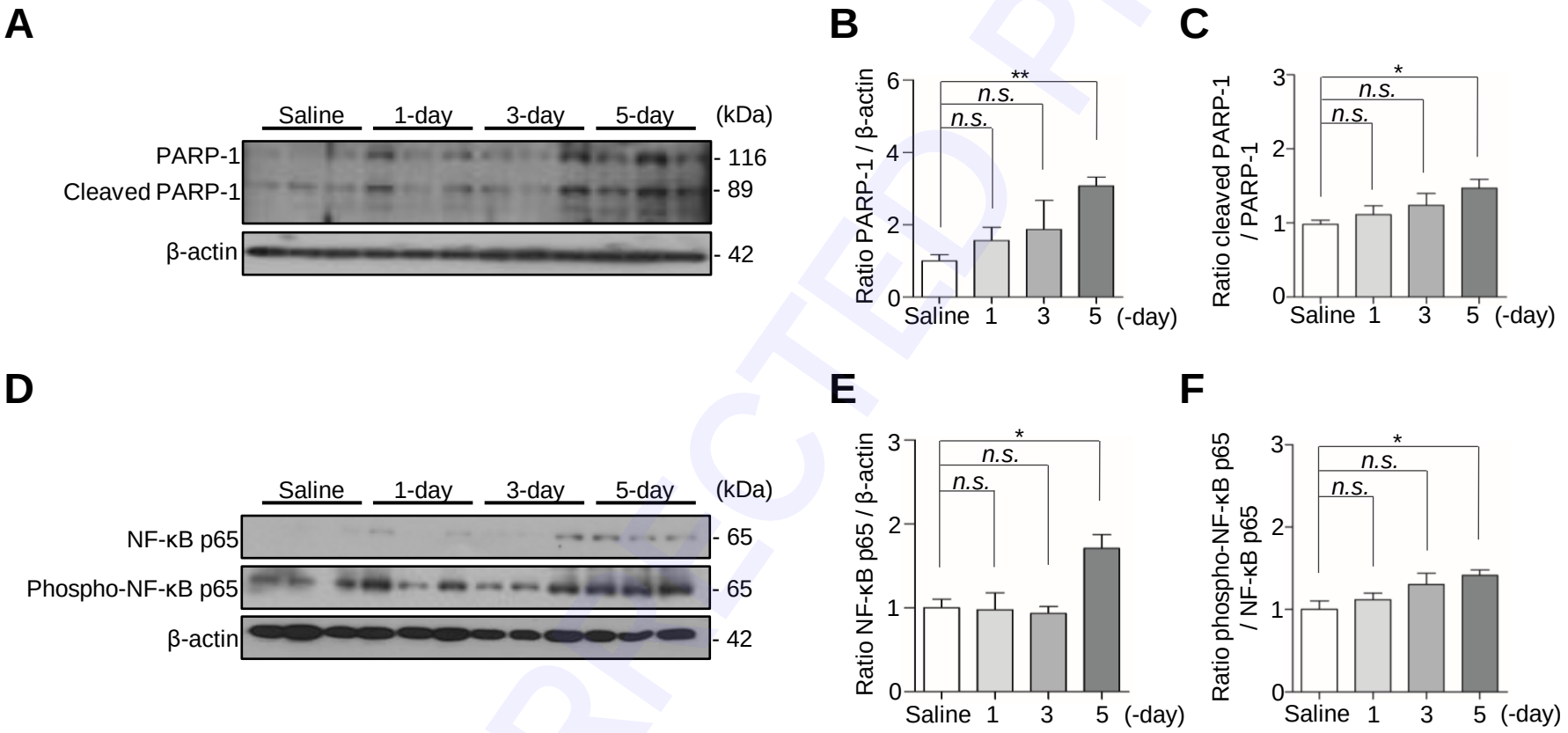

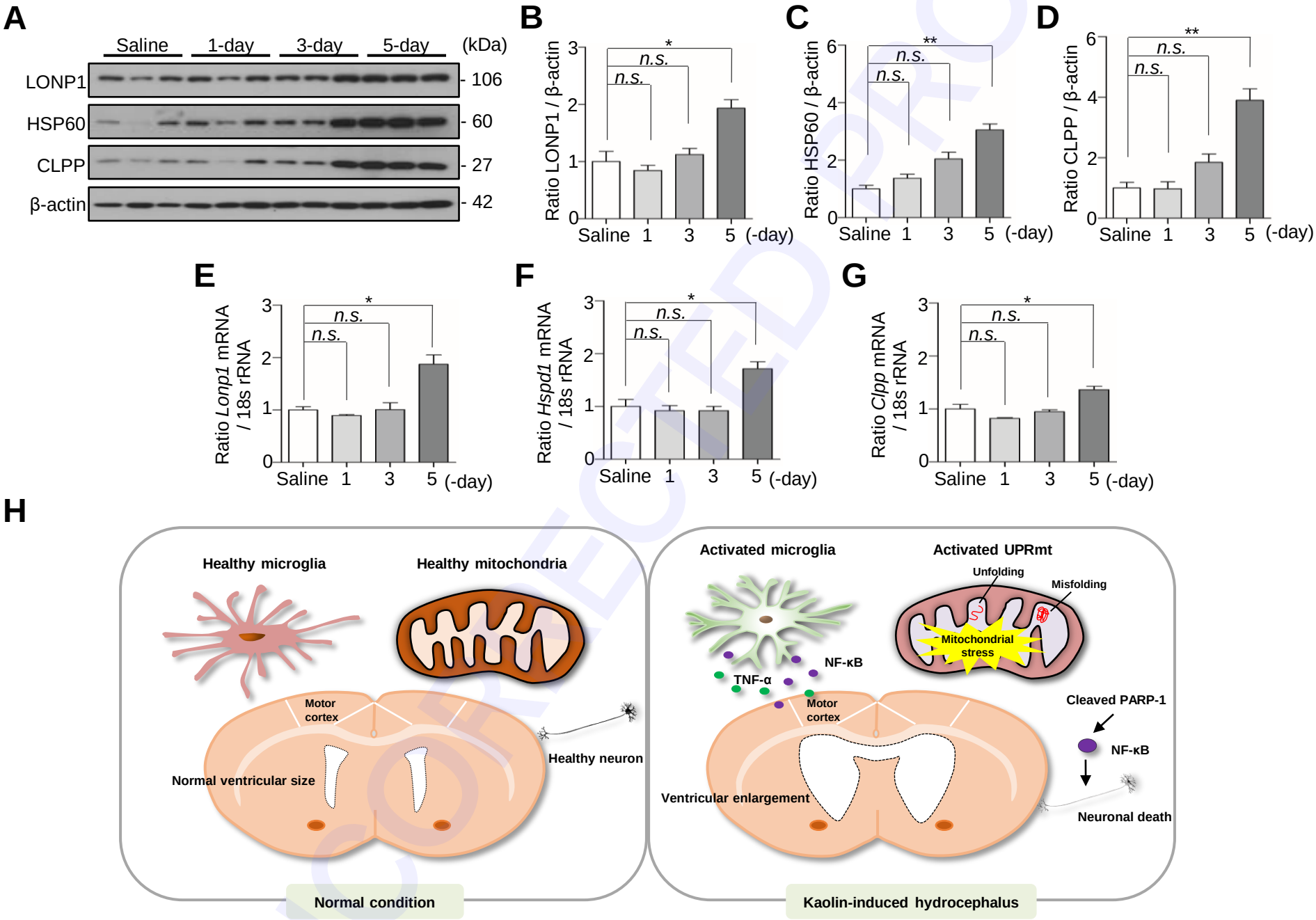
A
Saline
1-day
3-day
5-day
(kDa)
LONP1
HSP60
CLPP
β-actin
106
60
27
42
B
Ratio LONP1 / β-actin
C
Ratio HSP60 / β-actin
D
Ratio CLPP / β-actin
E
Ratio Lonp1 mRNA / 18s rRNA
F
Ratio Hspd1 mRNA / 18s rRNA
G
Ratio Clpp mRNA / 18s rRNA
n.s.
*
**
Saline 1 3 5 (-day)
H
Healthy microglia
Healthy mitochondria
Motor cortex
Healthy neuron
Normal ventricular size
Normal condition
Activated microglia
Activated UPRmt
Unfolding
Misfolding
Mitochondrial stress
NF-κB
TNF-α
Motor cortex
Cleaved PARP-1
NF-κB
Neuronal death
Ventricular enlargement
Kaolin-induced hydrocephalus

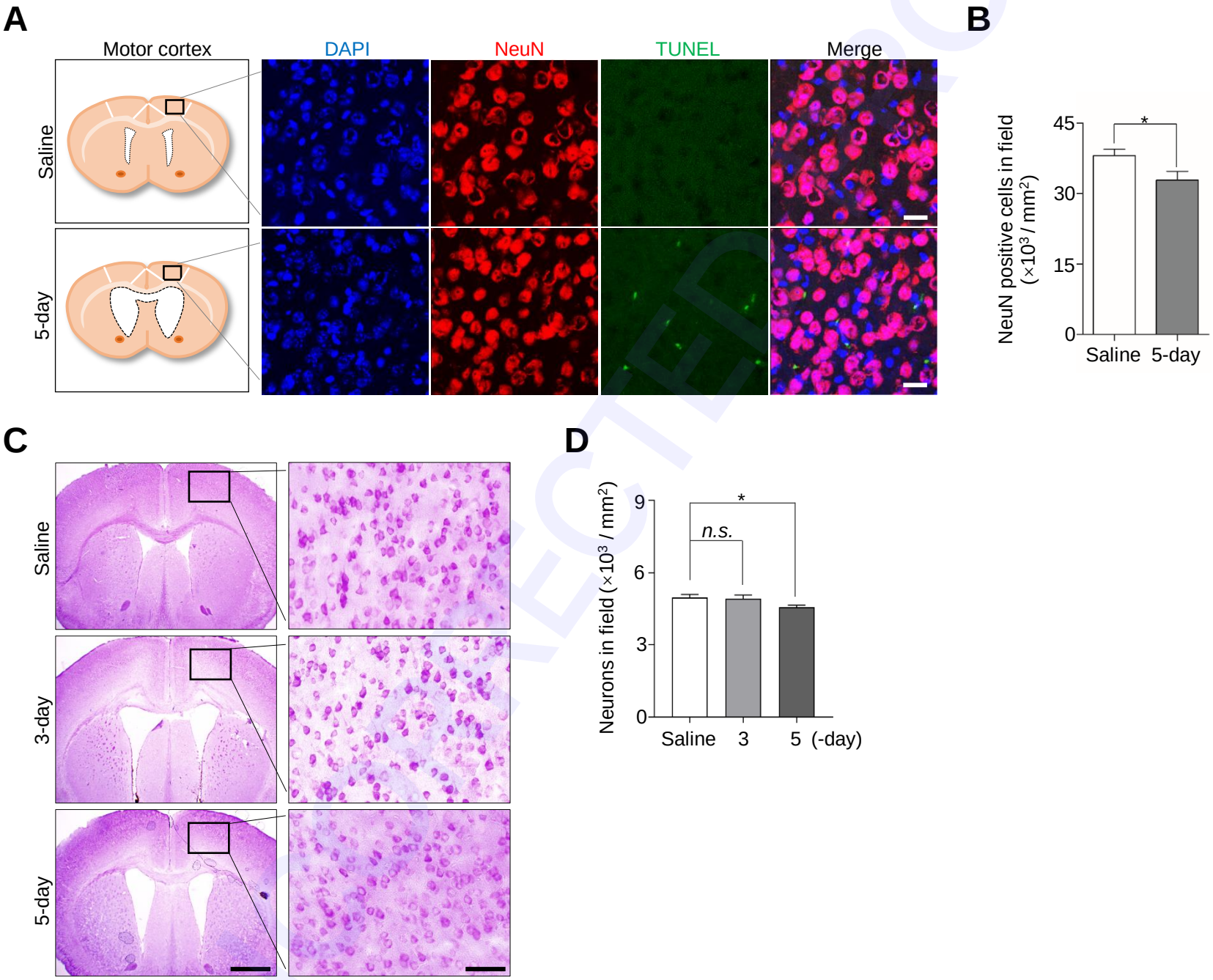

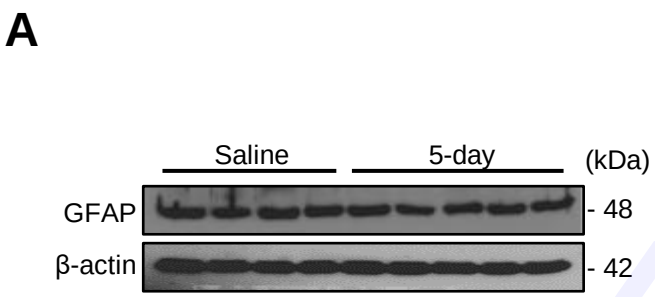

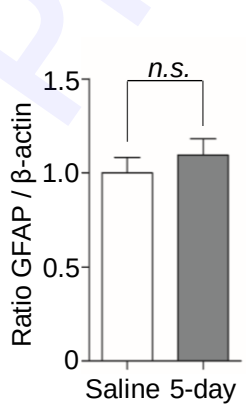

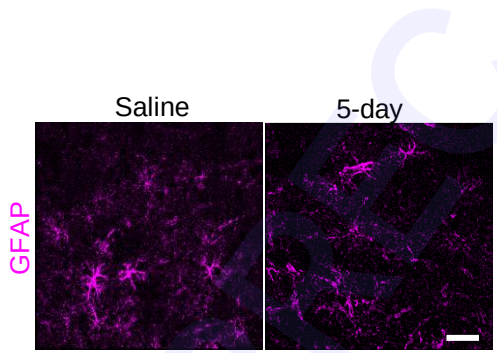

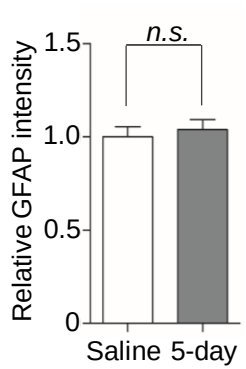

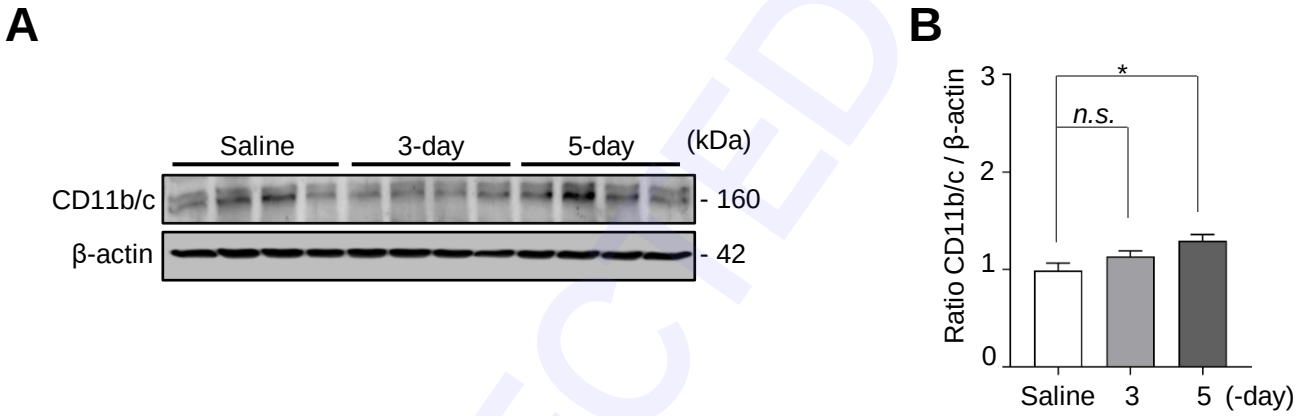

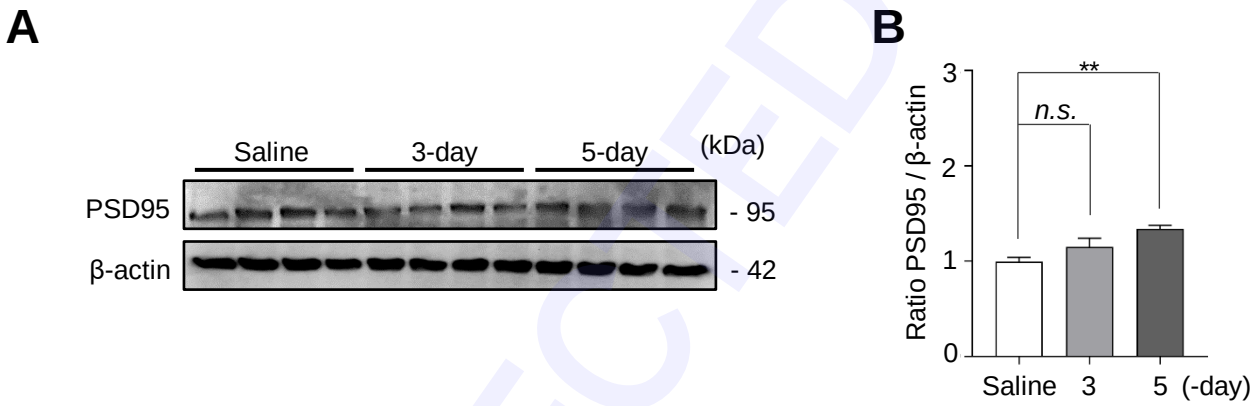

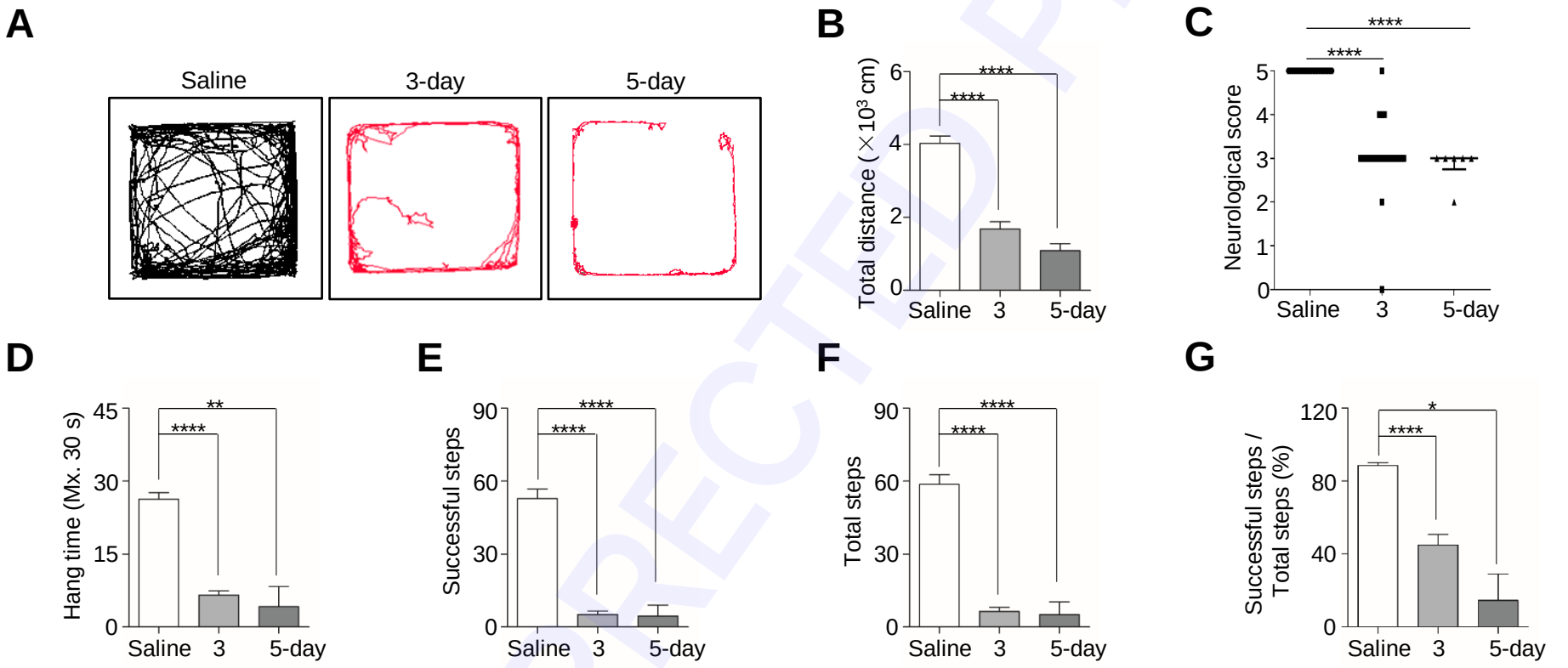

Supplemental figure 6

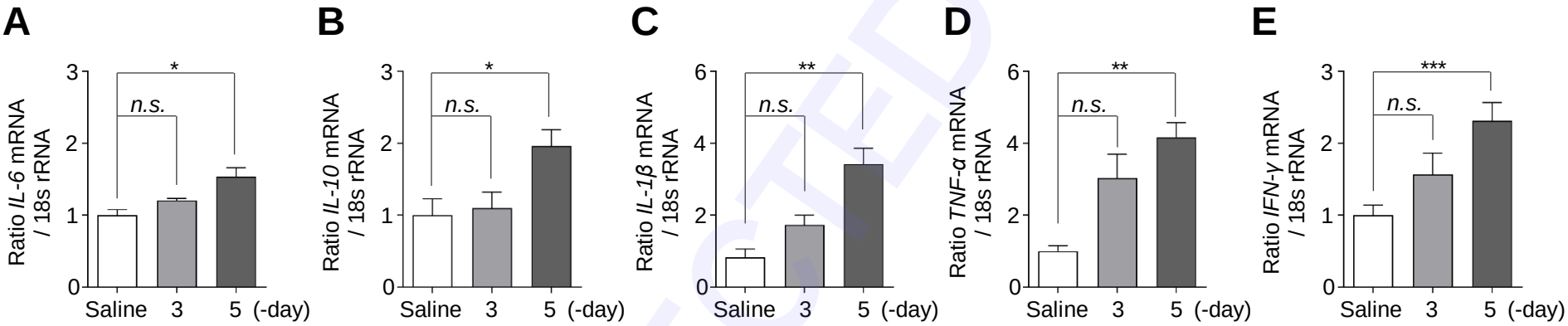

SUPPLEMENTAL MATERIALS

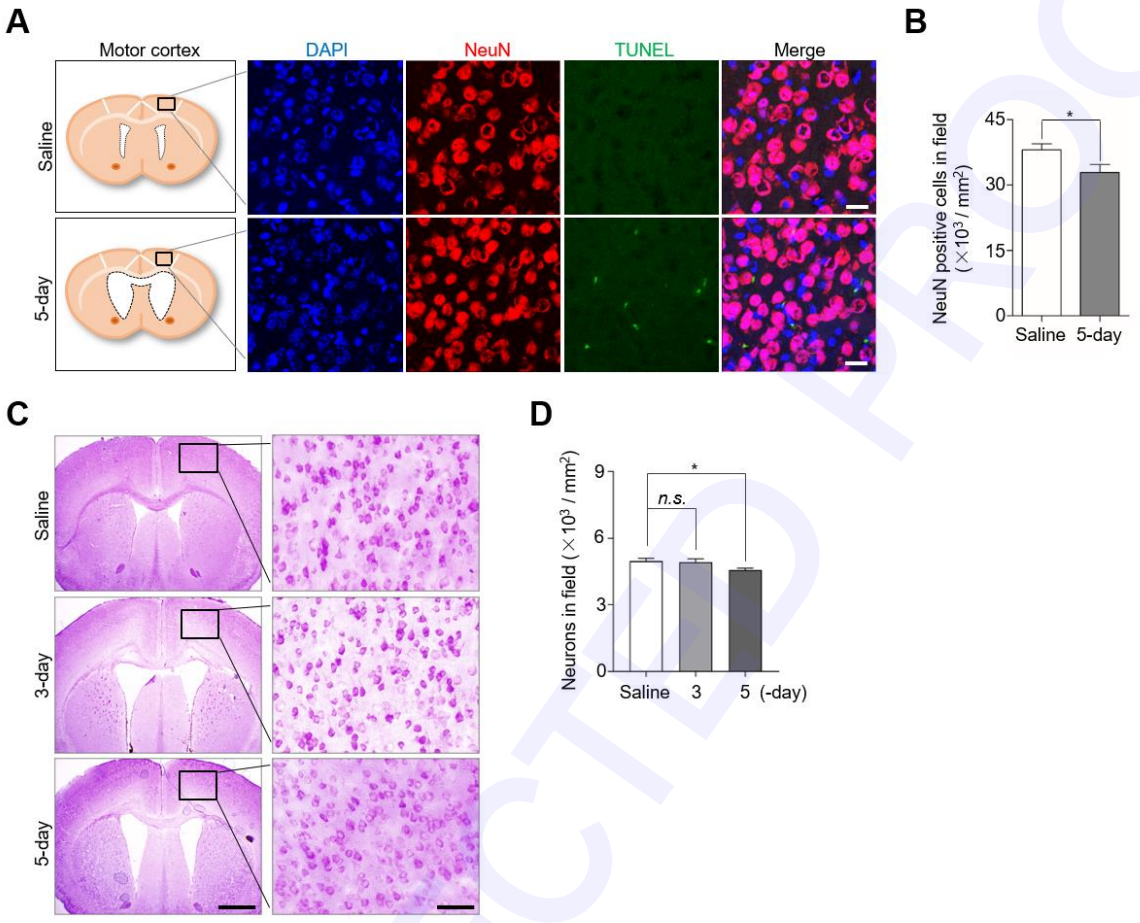

Supplemental fig. 1. The percentage of apoptotic neurons increased in the 5-day kaolin group. (A) The motor cortex above the ventricles was stained for DAPI (blue), NeuN (red), and TUNEL (green). (B) The NeuN positive cells in field were quantified, n = 6. (C) The motor cortex above the ventricles was stained by Nissl. (D) The neurons in field were quantified, n = 3 (* $P < 0.05$; n.s., not significant).

Scale bar: A: 20 μm, C: 200 μm, the enlarged images: 36 μm.

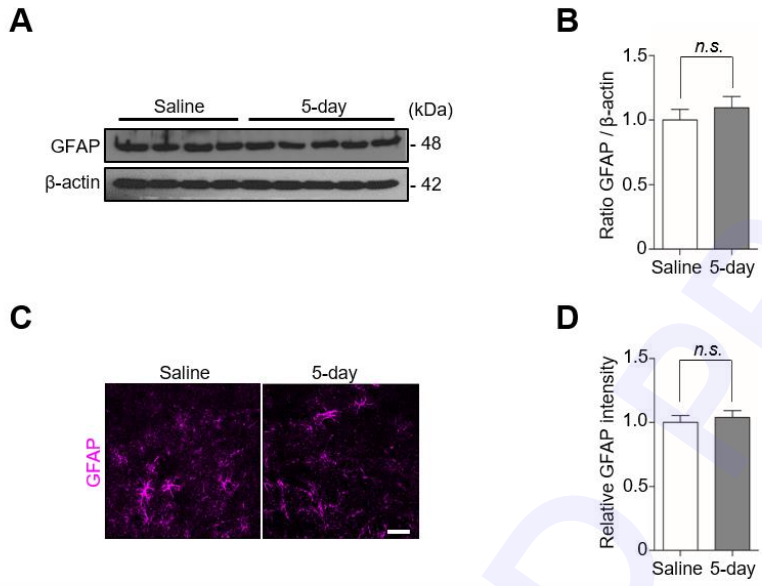

Supplemental fig. 2. The expression of astrocyte was not changed in the 5-day kaolin group. (A) The expression of GFAP in the motor cortex was analyzed by western blotting. (B) The intensity value of GFAP was shown. (C) The motor cortex was stained for the marker of astrocyte GFAP. (D) The immunofluorescence intensity of GFAP was quantified. Western blotting n (saline) = 4, n (5-day) = 5, immunofluorescence n = 5 (n.s., not significant). Scale bar: 20 μm.

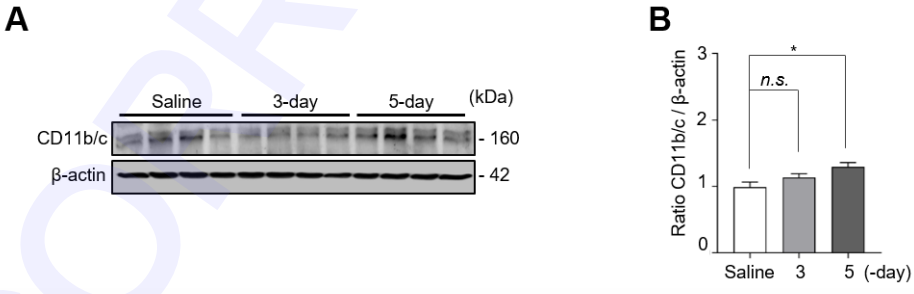

Supplemental fig. 3. Microglia activated in the 5-day kaolin group. (A) The expression of CD11b/c in the motor cortex was analyzed by western blotting. (B) The intensity value of CD11b/c was shown, n = 4 (* $P < 0.05$; n.s., not significant).

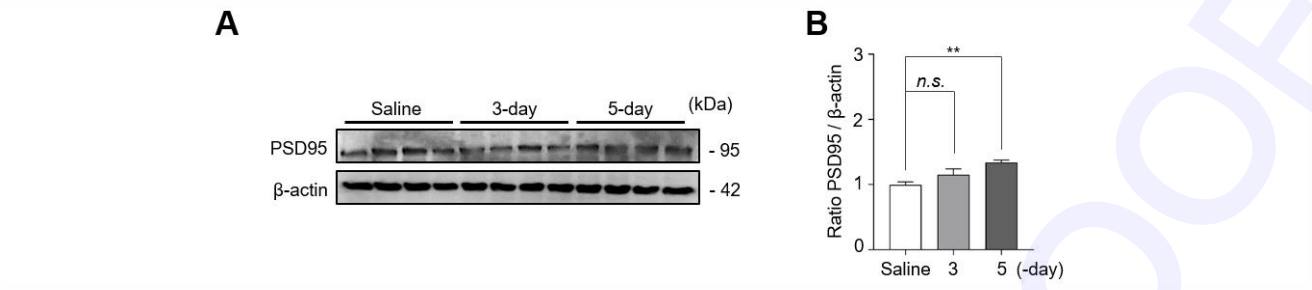

Supplemental fig. 4. PSD95 upregulated in the 5-day kaolin group. (A) The expression of PSD95 in the motor cortex was analyzed by western blotting. (B) The intensity value of PSD95 was shown, n = 4 (** P < 0.01; n.s., not significant).

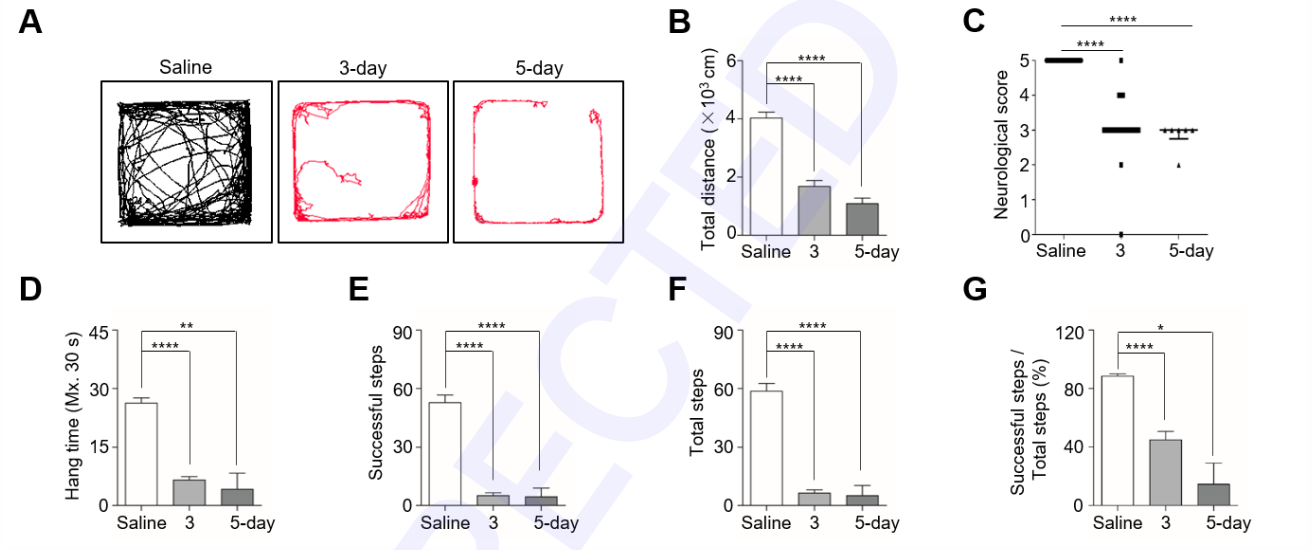

Supplemental fig. 5. Kaolin-induced hydrocephalus mice show motor disturbances in both 3-day and 5-day groups. (A, B) Movement activity was measured for 10 min in the open-field test. (C) The neurological function was scored by a 5-point paradigm and plotted. (D–G) Bar plots showed the results were calculated for 30 s in a horizontal grid test. Behavior test n (saline) = 16, n (3-day) = 24, and n (5-day) = 6. For the neurological score, n (3-day) = 24. For the open-field test and horizontal grid test, n (3-day) = 23 (* P < 0.05, ** P < 0.01, **** P < 0.0001).

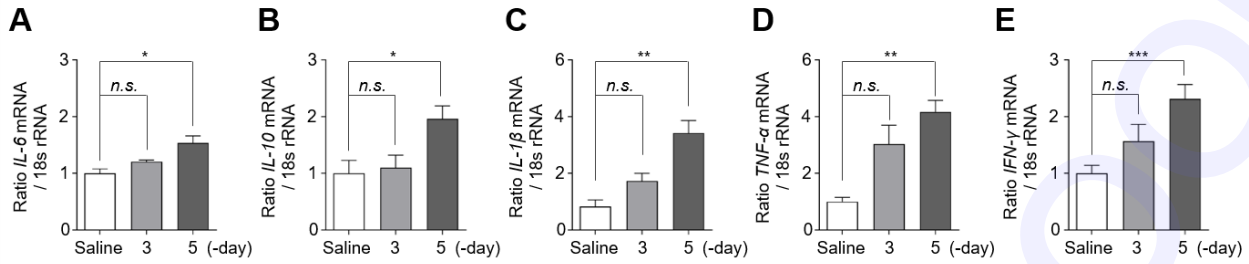

Supplemental fig. 6. Inflammatory cytokines expression increased in the 5-day kaolin group. (A–E) The expression of *IL-6, IL-10, IL-1β, TNF-α,* and *IFN-γ* in the motor cortex was analyzed by qPCR, n = 4 (* $P < 0.05$, ** $P < 0.01$, *** $P < 0.001$; n.s., not significant).

MATERIALS AND METHODS

Animals

Eight weeks old male C57BL/6J mice (Damul Science, Daejeon, Korea), provided with a standard chow diet (Research Diets, AIN-76A, New Brunswick, NJ, USA) and water *ad libitum*. Mice were maintained at 22°C, 12 h light/dark cycle (light phase: 6:00 to 18:00, dark phase: 18:00 to 6:00). All the experimental procedures were approved by the Institutional Animal Care and Use Committee of Chungnam National University (ethical approval number, 202103A-CNU-022).

Mice model of kaolin-induced hydrocephalus

The mouse head was fixed in the stereotactic frame (KOPF, CA), anesthetized with 2.5% sevoflurane (Ilsung, Seoul, Korea) in an O_2 air mixture (2:1) delivered by loosely snout mask, anesthesia was verified by touching the footpad. Wipers tissue to protect mouse eyes, 70% ethanol sterilized mouse head. Followed midline made 1 cm incision, separated the soft tissue and muscle, exposed the cisterna magna. In the saline group, cisterna magna was injected with 10 μL saline. In the kaolin group, cisterna magna was injected with 10 μL 25% kaolin (250 mg/mL in saline; Sigma, K7375), through a 0.5 mL

insulin syringe (Becton-Dickinson, 328821). After surgery, mice have sutured the muscle and skin, allowed to recover from anesthesia on a heated surface for 30 min. Returned the mice to their cages, kept them at room temperature, and provided them with standard chow and water *ad libitum*.

Measurement of ventricular size

Mice were randomly divided into 3 experimental groups, 6 mice per group: (a) saline group (the fifth day after 10 μL saline injection), (b) 1-day group (the first day after 10 μL 25% kaolin injection), (c) 3-day group (the third day after 10 μL 25% kaolin injection), and (d) 5-day group (the fifth day after 10 μL 25% kaolin injection). All the mice were euthanized with sevoflurane and then brains were collected. Mice brains were immersed in 4% paraformaldehyde for 48 h and dehydrated in 30% sucrose solution at 4°C for another 48 h. Then samples were frozen and sliced into coronal sections, from the anterior horn of the lateral ventricle (Lv) to the 4th ventricle (4v), the thickness of 100 μm using a cryotome (Leica). Slices were mounted on glass slides and imaged at 20 magnifications under a microscope (Olympus, Japan). The size of the Lv, the dorsal part of the 3rd ventricle (d3v), the ventral part of the 3rd ventricle (v3v), and the 4v were analyzed by the Image J software.

Behavioral analysis

Mice were randomly divided into 2 experimental groups: (a) 16 mice in the saline group (the third day after 10 μL saline injection), (b) 24 mice in the 3-day group (the third day after 10 μL 25% kaolin injection), and (c) 6 mice in the 5-day group (the fifth day after 10 μL 25% kaolin injection). Mice were handled 3 days before behavioral tests, to reduce the effects that handling stress might have on the tests. All tests were carried out from 9:00 to 18:00 during the light phase, in the same low-intensity lightroom, and analyzed by the same experimenter. After the test, mice were returned to their cage and the boxes were cleaned with 70% ethanol. EthoVision XT 11.5 software to analyze the mice behavior.

Open-field test

The general activity was recorded by placing the mice in a 40 × 40 × 40 cm box for 10 min. To start the test, a mouse was placed at the center of the box. And the travel distance was recorded.

Neurological score

Mice were scored for global neurologic function, using a modified neurological scale as follows: normal (5), decreased scavenging activity and scatter reflex (4), no spontaneous scavenging, loss of scattering reflex, ataxia (3), non-purposeful movements (2), loss of righting reflex (1), dead (0) (1).

Horizontal grid test

The hang time, successful steps, and total steps were recorded, by placing the mouse in a 12 × 12 cm horizontal square grid box. The box includes the bottom clear plexiglass walls, a height of 20 cm. The top black plexiglass walls, the height of 8 cm, with 0.8 × 0.8 cm wire mesh. Placed the grid side on the floor, put the mouse in the box. When the mouse grabbed the grids with four paws, the box inverted slowly, the mouse would hang on the grid. The camera recorded for 30 s and replayed the videos for analysis.

Immunofluorescence

Mice were randomly divided into 2 experimental groups, 6 mice per group: (a) saline group (the fifth day after 10 μL saline injection) and (b) 5-day group (the fifth day after 10 μL 25% kaolin injection). All the mice were euthanized with sevoflurane and then brains were collected. Mice were perfused and fixed with 4% paraformaldehyde and dehydrated with 30% sucrose solution at 4°C for 48 h. Then samples were frozen and sliced into coronal sections, at a thickness of 30 μm using a cryotome. The sections were stored in tissue stock solution and blocked in 2% donkey serum (Gene Tex), 0.3% Triton

X-100 with phosphate-buffered saline (PBS) for 1.5 h and then incubated with anti-TNF-α (1:100; Abcam, ab6671), ionized calcium-binding adaptor molecule-1 (Iba-1) (1:200; Novus Biologicals, NB100-1028), GFAP (1:600, Abcam, 4674), at 4°C overnight. Washed with PBS, and incubated Alexa Fluor® 488 AffiniPure Donkey Anti-Rabbit IgG (H+L) (1:100; Jackson Immuno, 711-545-152), Alexa Fluor® 594 AffiniPure Donkey Anti-Goat IgG (H+L) (1:200; Jackson Immuno, 705-585-147), Alexa Fluor® 647 AffiniPure Donkey Anti-Chicken IgG (H+L) (1:600; Jackson Immuno, 703-605-155) for 1.5 h at room temperature, Hoechst 33342 Trihydrochloride (1:5000; MedChemExpress, HY-15559A) for 3 min at room temperature. Using fluorescent mounting solution (Dako) mounted tissue on slides, imaged by the confocal microscope (Leica). Fluorescence integrated density (IntDen) was quantified with the Image J software.

ELISA measurements

Mice were randomly divided into 4 experimental groups, 6 mice per group: (a) saline group (the fifth day after 10 μL saline injection), (b) 1-day group (the first day after 10 μL 25% kaolin injection), (c) 3-day group (the third day after 10 μL 25% kaolin injection), and (d) 5-day group (the fifth day after 10 μL 25% kaolin injection). All the mice were euthanized with sevoflurane and then brains were collected. The motor cortex above the ventricles was homogenized in 200 μL PBS, centrifuged at 3000 rpm for 5 min at 4°C. The supernatants were stored at -70°C until performed mouse TNF-α enzyme-linked immunosorbent assay (ELISA) (KOMA, K0331186) according to the manufacturer's instructions.

Western blotting

Mice were randomly divided into 4 experimental groups, 3 mice per group: (a) saline group (the fifth day after 10 μL saline injection), (b) 1-day group (the first day after 10 μL 25% kaolin injection), (c) 3-day group (the third day after 10 μL 25% kaolin injection), and (d) 5-day group (the fifth day after

10 μL 25% kaolin injection). All the mice were euthanized with sevoflurane and then brains were collected. The motor cortex above the ventricles was separated and lysed by radioimmunoprecipitation assay (RIPA) buffer with phosphatase inhibitor and protease inhibitor cocktail (Roche) to extract the protein. The extracted protein (each 20 μg protein) was run on sodium dodecyl sulfate-polyacrylamide gel electrophoresis (SDS-PAGE) and then were transferred to polyvinylidene fluoride (PVDF) membrane (Millipore). The PVDF membranes were blocked with 2.5% bovine serum albumin (BSA) (GenDEPOT) for 1 h at room temperature, then incubated 4°C, overnight with anti-TNF-α (1:1000; Abcam, ab6671), p65 (1:500; Cell Signaling Technology, 8242), phosphorylated p65 (P-p65) (1:500; Cell Signaling Technology, 3033), Iba-1 (1:500; Novus Biologicals, NB100-1028), LONP1 (1:1000; Abcam, 103809), HSP60 (1:5000; Abcam, 46798), CLPP (1:1000; Sigma, HPA010649), PARP-1 (1:1000; Cell Signaling Technology, 9532), GFAP (1:5000, Abcam, 7260), CD11b/c (1:500, Neuromics, RA25012), PSD95 (1:2000, Thermo, MA1-046), and β-actin (1:2000; Santa Cruz Biotechnology, sc-47778) in 1% BSA. The PVDF membranes were washed with Tris-buffered saline with Tween (TBST) and incubated with secondary antibodies IgG horseradish peroxidase antibody (HRP, Pierce Biotechnology), for 1.5 h at room temperature. The protein band was visualized by the enhanced chemiluminescence (ECL) reagent (Thermo). Then used medical X-ray film blue (AGFA CP-BU NEW), developer solution, and fixer solution for the ECL detection. Band intensity was quantified with the Image J software.

TUNEL staining

Mice were randomly divided into 2 experimental groups, 6 mice per group: (a) saline group (injected with 10 μL saline as vehicle solution) and (b) 5-day group (the fifth day after 10 μL 25% kaolin injection). All the mice were euthanized with sevoflurane and then brains were collected. The brain tissues were embedded in 4% paraformaldehyde, dehydrated brain sections were stained with terminal-

deoxynucleotidyl transferase-mediated nick end labeling (TUNEL) assay (Roche, 11684795910) according to the manufacturer's instructions. Double-label with neuronal nuclear antigen (NeuN) (1:200; Abcam, ab104224). Finally, the sections were covered with 4'6-diamidino-2-phenylindole (DAPI) (1:5000; Thermo, H3570). The slides were imaged using the confocal microscope (Leica). Fluorescence IntDen was quantified with the Image J software.

Nissl staining

Mice were randomly divided into 3 experimental groups, 3 mice per group: (a) saline group (injected with 10 μL saline as vehicle solution), (b) 3-day group (the third day after 10 μL 25% kaolin injection), and (c) 5-day group (the fifth day after 10 μL 25% kaolin injection). All the mice were euthanized with sevoflurane and then brains were collected. The brain tissues were embedded in 4% paraformaldehyde, dehydrated brain sections were stained with 0.1% cresyl violet for 3 min, dehydrated through graded alcohols (70, 95, 100%). Using fluorescent mounting solution (Dako) mounted tissue on slides, imaged by the confocal microscope (Leica). Neurons in field were quantified with the Image J software.

Quantitative Real-time PCR (qPCR)

Mice were randomly divided into 4 experimental groups, 3 mice per group: (a) saline group (the fifth day after 10 μL saline injection), (b) 1-day group (the first day after 10 μL 25% kaolin injection), (c) 3-day group (the third day after 10 μL 25% kaolin injection), and (d) 5-day group (the fifth day after 10 μL 25% kaolin injection). Total RNAs were isolated by TRIzol reagent (Thermo) and cDNA was prepared with reverse transcription master premix (5 × Rnase H+). The qPCR was performed with cDNA, SYBR green PCR master mix (PhileKorea, Korea), and primers. *Lonp1* primer (Forward: 5`-GACAGAGAACCCGCTAGTGC-3`, Reverse: 5`-CTCAGTGGTTCTGGGATGGT-3`), *Hspd1* primer (Forward: 5`-GAGCTGGGTCCCTCACTCG-3`, Reverse: 5`-AGTCGAAGCATTTCTGCGGG-3`), *Clpp* primer (Forward: 5`-GCCATTCACTGCCCAATTCC-3`,

Reverse: 5`-TGCTGACTCGATCACCTGTAG-3`), *IL-6* primer (Forward: 5`-ACAACCACGGCCTTCCCTACTT-3`, Reverse: 5`-CACGATTTCCCAGAGAACATGTG-3`), *IL-10* primer (Forward: 5`-ATAACTGCACCCACTTCCCA-3`, Reverse: 5`-GGGCATCACTTCTACCAGGT-3`), *IL-1β* primer (Forward: 5`-TGACGGACCCCAAAAGATGA-3`, Reverse: 5`-AAAGACACAGGTAGCTGCCA-3`), *TNF-α* primer (Forward: 5`-CCCACGTCGTAGCAAACCAC-3`, Reverse: 5`-GCAGCCTTGTCCCTTGAAGA-3`), *IFN-γ* primer (Forward: 5`-AGACATCTCCTCCCATCAGCAG-3`, Reverse: 5`-TAGCCAAGACTGTGATTGCGG-3`), and *18s rRNA* primer (Forward: 5′-CGACCAAAGGAACCATAACT-3′, Reverse: 5′-CTGGTTGATCCTGCCAGTAG-3′). Results were analyzed with the Rotor-Gene 6000 real-time rotary analyzer system (Corbett Life Science).

Statistical analysis

All results are acquired from at least three independent experiments and are presented as the mean ± SEM. Data were compared using a student's *t*-test or a one-way ANOVA (Prism software). P-values < 0.05 were deemed statistically significant.

Reference:

1. Bloch O, Auguste KI, Manley GT and Verkman AS (2006) Accelerated progression of kaolin-induced hydrocephalus in aquaporin-4-deficient mice. J Cereb Blood Flow Metab 26, 1527-1537